CHEMICAL ENGINEERING TRANSACTIONS
VOL. 103, 2023
A publication of AIDIC
The Italian Association of Chemical Engineering
Online at www.cetjournal.it
Guest Editors: Petar S. Varbanov, Panos Seferlis, Yee Van Fan, Athanasios Papadopoulos

ISBN 979-12-81206-02-1; **ISSN** 2283-9216
DOI: 10.3303/CET23103056

Parameter Sensitivity Analysis and Optimization of Nickel-Iron Batteries Using a Physics-Based Model

Hui-ju C. Chuang, Patricia Kei Y. Tanate, Justine Marie E. Abarro, Julie Anne D.R. Paraggua*

Laboratory of Electrochemical Engineering, Department of Chemical Engineering, University of the Philippines Diliman, Quezon City 1101, Philippines
jddelrosario2@up.edu.ph

Large-scale energy storage has rapidly advanced with the increasing demand for clean energy sources. One type of storage is the nickel-iron (Ni-Fe) battery which is regaining attention due to its cost-effectiveness, durability, and inherent safety. However, its full capability is limited by its low energy and power density due to low active iron utilization and Coulombic efficiency due to hydrogen formation at the anode. While most research on improving Ni-Fe batteries focused on experimental studies, multiphysics modeling is a practical tool to analyze the phenomena in the battery system instead. This study built a simple one-dimensional (1D) isothermal multiphysics model of a Ni-Fe battery with nanostructured electrodes using COMSOL Multiphysics®. Sensitivity analysis was conducted based on the first discharge plateau only (1-step case) and on the overall discharge (2-step case) to investigate the susceptibility of energy density to battery design parameters. These parameters were ranked according to their sensitivity and subjected to a constrained optimization by linear approximation (COBYLA) algorithm to optimize the energy and power density. In the 1-step case, the simultaneous optimization resulted in a ~ 25 % increase in energy density and a ~ 23 % increase in power density, which correspond to the maximized anode thickness and minimized cathode porosity. Results in the 2-step case showed a ~ 23 % increase in energy density and an ~ 18 % increase in power density, which are attributed to the minimization of cathode thickness, porosity, and active particle size.

1. Introduction

The nickel-iron battery (Ni-Fe) is known for its long operating life, high theoretical specific capacity, and good tolerance for electrical abuse (Linden et al., 2019). However, the electrode reactions limit its widespread use. Oxidation of the Fe electrode involves a series of chemical reactions forming a passivation layer of poorly conductive iron oxides on the electrode surface, reducing the battery capacity (Periasamy, 1996). The inherent hydrogen evolution reaction (HER) during charging also lowers the efficiency. Addressing these limitations, Hongjie Dai's group improved the rate performance and mitigated passivation by incorporating graphitic nanocarbon with active materials, producing novel hybrid electrodes (Wang et al., 2012). Consequently, this led to extensive research on Ni-Fe batteries focusing on optimizing the electrode composition and morphology and modifying the electrolyte composition (He et al., 2021). Tang et al. (2019) demonstrated that the facile spray drying method is a convenient alternative to the conventional high-pressure hydrothermal synthesis for producing a uniform carbon coating on the active material for industrial applications. However, research on Ni-Fe batteries, involving material investigation, design parameter adjustment, and exploration of facile methods, often incurs high costs and requires iterative work to achieve desired outcomes. In this regard, experimental limitations on alkaline batteries can be overcome by using multiphysics models that predict system behavior under various conditions (Castro et al., 2022). However, modeling studies specific to Ni-Fe batteries are inadequately explored, with only one identified thermal modeling study conducted by Lee et al. (1986). Raventos et al. (2021) developed a 'battolyser', integrating a Ni-Fe battery and an alkaline electrolyzer. Using a 1D COMSOL Multiphysics model, they simulated the electrochemical reactions to optimize electrode parameters. To fully capture the governing electrochemical

Paper Received: 14 April 2023; Revised: 29 May 2023; Accepted: 14 June 2023
Please cite this article as: Chuang H.-J.C., Tanate P.K.Y., Abarro J.M.E., Paraggua J.A.D., 2023, Parameter Sensitivity Analysis and Optimization of Nickel-Iron Batteries Using a Physics-Based Model, Chemical Engineering Transactions, 103, 331-336 DOI:10.3303/CET23103056

reaction, kinetics, and transport phenomena in the battery system, this study developed a 1D isothermal multiphysics model of a Ni-Fe battery to determine the optimum energy density and power density through sensitive design parameters. Models based on other battery systems with similar mechanisms—like lead-acid and nickel-cadmium (Ni-Cd) batteries—were used as references. For instance, both lead-acid and Ni-Fe batteries operate in flooded configuration, inherently encounter HER, and suffer from electrode passivation through a dissolution-precipitation mechanism. Despite the correlation, evaluating how such a model can accurately represent Ni-Fe chemistry is still necessary. Furthermore, the developed model was validated by comparing simulation results with the experimental data obtained by Lei et al. (2016).

2. Methodology

2.1 Multiphysics modeling

A simple 1D isothermal multiphysics model of a Ni-Fe battery was built using the COMSOL Multiphysics®. All pertinent design parameter information was based on the experimental set-up of Lei et al. (2016). The model geometry is arranged in such order: negative electrode, electrolyte layer, separator, another electrolyte layer, and positive electrode. It is composed of Fe/multiwalled carbon nanotubes (MWCNT) anode and NiO/MWCNT cathode in 8 M KOH electrolyte with a Celgard 3401 separator, discharged at 200 mA/g. The effective conductivities for both electrodes were assigned a fixed value of 100 S/cm. The parameters for the model development are listed in Table 1. To determine the analysis range of the parameter reference values, four points equally spaced and different from the reference value were chosen. These ranges were crosschecked with commonly reported values in the existing literature to ensure practical results. As for electrode porosities, only two points were considered during the analysis, while nine points were considered for electrolyte concentration for a wider scope. With the range of acceptable parameters, a one-at-a-time parametric sweep was done for each input parameter. The model was validated by comparing the root mean square error (RMSE) of the discharge curve from the experimental data of Lei et al. (2016). For the model to be considered accurate and a good fit, the computed RMSE must be small enough relative to the data that was obtained.

Table 1: Ni-Fe battery kinetic and transport parameters

Parameter	Anode	Separator	Electrolyte	Cathode
Thickness [cm]	0.05 (± 40 %) [a]	0.0025 (± 40 %) [b]	0.05 [*,†]	0.05 (± 40 %) [a]
Porosity	0.731 (-0.10) [*]	0.41 (±0.20) [b]		0.84908 (-0.10) [*]
Particle size [nm]	1,000 (±30 %) [*]			1,330 (±30 %) [*]
Active material loading [mg/cm^2]	5 (± 60 %) [a]			10 (± 60 %) [a]
Equilibrium potential vs. Hg/HgO [V]	-0.9783 [c]			0.3517 [c]
Transfer coefficient	0.5 [d]			
Exchange current density [A/cm^2]	5.47x10^{-4} [a]			1.09x10^{-3} [a]
Concentration [mol/L]			8 (1-10) [a]	

[a] (Lei et al., 2016), [b] (Tsehaye et al., 2021), [c] (Linden et al., 2019), [d] (De Vidts & White et al., 2019), [*] Calculated based on the experimental data of Lei et al. (2016), [†] Considered one side of the separator; multiply by 2 for actual thickness.

2.2 Parameter sensitivity analysis and optimization

The parameter influence on battery performance was determined through a sensitivity analysis method proposed by Jiang et al. (2020). The eleven design parameters investigated include electrode thickness, electrode active material loading, electrode particle size and porosity, separator thickness, separator porosity, and electrolyte concentration. Using the experimental data as a reference value, an acceptable range of values from the available literature was determined, as presented in Table 1. Four different points, x_n (n = 1, 2, 3, 4), within the specified range but not equal to the initial value of a parameter (experimental data), x_0, were estimated using the determined analysis range to calculate the rate of change of the value during parameter analysis, X_n, as shown in Eq(1). The sensitivity of the parameter, M, with respect to current density, i, was calculated using Eq(2), where $g_i(x)$ is the energy density of the battery when the parameter is x, $G_i(x)$ is the change ratio of the objective function of the battery when the model calculates the parameter x, and k is the number of parameter values. The obtained values were categorized depending on the following sensitivity conditions: M values less than 0.01 are classified as ‘insensitive’, while M values greater than or equal to 0.5 are classified as ‘very sensitive’. Any value in between is classified as ‘sensitive’. The design parameters were ranked according to their sensitivity and subjected to parameter optimization. However, in the case where only

a few parameters were classified as ‘very sensitive’, parameters that were ‘sensitive’ were also included. The gravimetric energy density, *E* (Wh/kg), and the power density, *P* (W/kg), at each condition were calculated as shown in Eq(3) and Eq(4). Lei et al. (2016) performed chronopotentiometry or galvanostatic method to estimate the experimental discharge capacity. The discharge current, *I*, is set in a steady-state behavior while the discharge voltage, *V(t)*, varies with time. The high current density effects over time were assumed to be negligible due to the relatively low discharge current density used in the reference study. The estimated energy and power densities were expected to be considerably greater than the experimental values since only the mass of active anode materials, *m* (mg/cm^2), was considered.

$$X_n = \frac{x_0 - x_n}{x_0} \tag{1}$$

$$M_i = \sqrt{\frac{1}{k}\sum_{n=1}^{k}\left[\frac{\left(\frac{g_i(x_0) - g_i(x_n)}{g_i(x_0)}\right)}{X_n}\right]^2} \tag{2}$$

$$E = \frac{1}{m}\int_0^t IV(t)dt \tag{3}$$

$$P = \frac{1}{mt}\int_0^t IV(t)dt \tag{4}$$

Optimization of battery design was implemented using the built-in optimization module of COMSOL Multiphysics® which is the constrained optimization by linear approximations (COBYLA) algorithm. The COBYLA method improves the accuracy of the results by iterative approximation of the actual constrained optimization problem. It is important to determine whether the optimization aims to minimize or maximize the objective function. In this case, the objective function, which is the energy density, was maximized.

3. Results and discussion

3.1 Model development and validation

In a typical discharge curve for a Ni-Fe battery, the first plateau occurring at 1.4–1.3 V vs standard hydrogen electrode (SHE) corresponds to the Fe^0 oxidation to Fe^{2+}, while the second plateau at 1.1–1.0 V vs SHE indicates further oxidation of Fe^{2+} to Fe^{3+} (Shukla et al., 1994). In most studies, only the first reaction is exploited and the succeeding step, which occurs under deep-discharge conditions, is of no practical importance (Linden et al., 2019). However, the sensitive parameters concerning both the 1-step and 2-step cases were still subjected to parameter optimization to acquire a complete overview. Figure 1 compares the discharge curve of the experimental data of Lei et al. (2016) and the simulated COMSOL model. The open-circuit voltage (OCV) of the simulation at 1.57 V shows a distinct deviation from the experimental discharge, which begins at 1.45 V. The second reaction occurs when the battery is over-discharged at the ~1.1V mark and the final discharge capacity of ~410 mAh/g_{Fe} happens at 1.0 V. Several factors unaccounted for in this model may also contribute to such deviation. These factors include temperature, conducting agent, binder, Bi_2S_3 electrode additive, or impurities in each component.

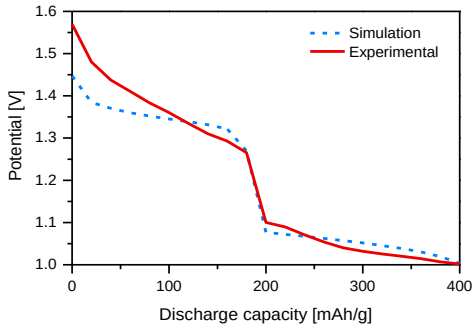

Figure 1: Comparison of the experimental vs simulated discharge curves of a Ni-Fe battery

Since the model was formatted based on an existing Ni-Cd model, it does not consider the actual state of charge (SOC), nor was it mentioned in the reference study as it makes use of the porosity variation. The computed RMSE value and the greatest absolute difference between the model and the experiment (∆max) voltages are 0.0417 V and 0.1225 V. With the significantly small RMSE values, the produced model is considered to be reliable despite having a large ∆max. The ∆max is directly attributed to the large OCV discrepancy between the model and experimental result, which consequently affects the overall RMSE. Voltage deviations observed throughout the simulated discharge curve also contribute to the calculated RMSE. Despite these deviations, the model still provides a good approximation of the discharge profile. The OCV value of the model falls within the range of 1.3–1.4 V, as reported by Shukla et al. (1994).

3.2 Parameter sensitivity analysis and optimization

Sensitivity analysis was conducted in two ways: (1) on the first plateau alone (1-step case), and (2) on the overall graph (2-step case). A parametric sweep was then performed for each parameter at the following discharge current densities: 150 mA/g, 200 mA/g (actual), and 250 mA/g. At varying current densities, minimal differences in the parameters observed can be considered insignificant. From the 11 factors initially considered, the very sensitive (VS) parameters for the 1-step and 2-step cases were identified and ranked as shown in Table 2. Anodic properties are prominent parameters for energy density at the first plateau, which describe the Fe oxidation to $Fe(OH)_2$. At the second plateau, the nickel reduction may compete with the $Fe(OH)_2$ oxidation as both reactions occur at the same potential range. The nickel hydroxide reduction occurs at 0.52 V vs. SHE (Shukla et al., 1994). The $Fe(OH)_2$ oxidation, on the other hand, occurs at –0.56 V vs SHE (Linden et al., 2019). This indicates that the cathodic parameters significantly influence the second plateau. The shift in the limiting parameters is caused by the nickel reaction kinetics, where the proton diffusion process affects the active material utilization (De Vidts and White, 1995).

Table 2: Five most sensitive parameters identified and ranked per plateau at 200 mA/g.

1-step case (1st plateau only)	M	2-step case (2 plateaus)	M
Porosity of anode (VS)	3.5459	Porosity of cathode (VS)	5.7762
Thickness of anode (VS)	0.7694	Particle size of cathode (VS)	1.1225
Active material loading of anode	0.1564	Thickness of cathode (VS)	0.8813
Electrolyte concentration	0.0730	Electrolyte concentration (VS)	0.5002
Porosity of cathode	0.0567	Porosity of anode	0.2398

In a Ragone plot, the energy density and power density show a consistent inverse relationship when varying the electrode thickness, electrode porosity, cathode particle size, and electrolyte concentration (Figure 2). Through a one-at-a-time parametric sweep, the energy density of the model demonstrates a high response to certain sensitive parameters such as the thickness and porosity of anode and electrolyte concentration. In most cases, the parametric value is directly proportional to energy density. Particularly, a thicker anode and concentrated KOH electrolyte result in a higher stable energy density (Figures 2a and 2f). By comparing the electrode thickness, as shown in Figures 2a and 2b, it can be confirmed that energy density is anode limited. Higher electrolyte concentration is also favorable as electrolyte conductivity is enhanced with more OH^- ions available for transport between the electrodes during the charge-discharge process. However, concentrations that are too high may also promote corrosion, resulting in a reduced life cycle and electrode swelling (Bernard, 2009). On the other hand, the enhanced performance at lower minimum porosities could be attributed to the $Fe(OH)_2$ accumulation on the electrode surface. The results align with other battery sensitivity studies where parameters such as electrode thickness, porosity, and particle size are among the most sensitive parameters, while separator-related parameters are among the least sensitive (Jiang et al., 2020).

Battery design optimization was conducted for both 1-step and 2-step cases through the COBYLA method while maintaining discharge time with the set constraints (Table 3). Design constraints were calculated using Lei et al.'s experimental work as set parameters (Table 1) to ensure that the optimized parameters resulted in higher energy and power density. In the 1-step case, the calculated lower bounds for the energy and power density at a 1 h discharge limit were set to 217.35 Wh/kg and 220 W/kg. Similarly, the calculated constraints for the 2-step case were ≥403.04 Wh/kg and ≥200 W/kg at a maximum discharge time of 2.1 h. The energy and power density values are based on the calculated values before optimization. A significant increase in thickness and decrease in active material loading of the anode is required to achieve improved energy and power density in the 1-step case. This inverse correlation indicates that increasing the active material loading is counterintuitive, emphasizing the importance of active material distribution on large surface area. As for the 2-step case, enhanced performance is attributed to the porosity, particle size, and thickness of the cathode.

The lower porosity implies enhanced electronic conductivity due to a greater active material fraction per unit mass of the cathode. A cathode with small particle size is also recommended because it provides shorter diffusion paths and larger specific surface areas, which promotes reactivity and active material accessibility (Rai et al., 2013). Lastly, cathode thickness had the largest reduction among other parameters to minimize the overall cell weight while achieving favorable active material utilization. Changes in other parameters were observed to be insignificant. Thus, the original value is retained and considered sufficient. However, it does not necessarily contradict the sensitivity analysis result. Several reasons why this might occur include the proximity of the initial parameter value to the optimal value, the competing effect of other parameters, or the limitations of the optimization algorithm used in terms of convergence criteria.

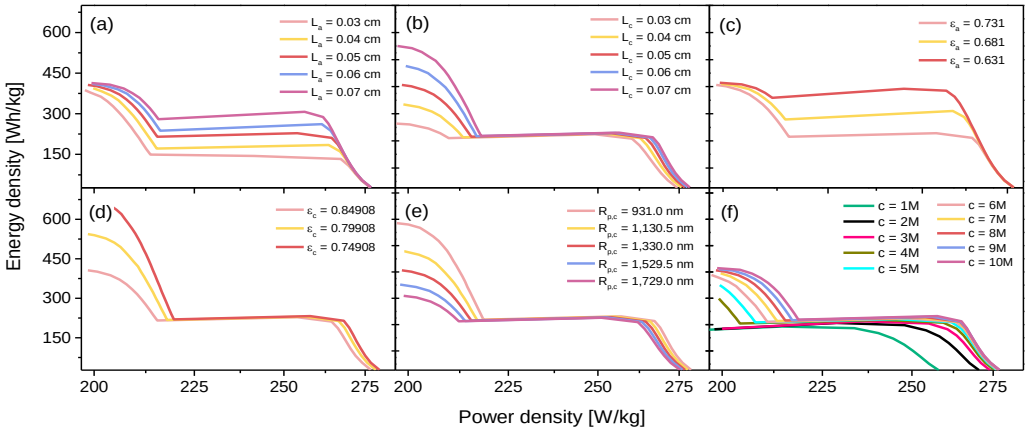

Figure 2: Ragone plots of the six most sensitive parameters at 200 mA/g: a) anode thickness (L_a), b) cathode thickness (L_c), c) anode porosity (ε_a), d) cathode porosity (ε_c), e) cathode particle size ($R_{p,c}$), f) electrolyte concentration

Table 3: Initial value and optimization results based on the COBYLA optimization method with energy density as the objective function for the 1-step and 2-step case

Case	Parameter	Initial value	Optimized value	% Difference
1-step	Minimum porosity of anode	0.731	0.731	0.00
	Thickness of anode [cm]	0.05	0.05238	4.76
	Active material loading of anode [mg/cm^2]	5	2	-60.00
	Electrolyte concentration [M]	8	8.0278	0.35
	Porosity of cathode	0.84908	0.81729	-3.74
	Energy density [Wh/kg]	217.3540	270.37	24.40
	Power density [W/kg]	220	270.37	22.90
	Discharge time [h]	0.98797	1.00000	1.22
2-step	Porosity of cathode	0.84908	0.84084	-0.97
	Particle size of cathode [nm]	1,330	1,269.9	-4.52
	Thickness of cathode [cm]	0.05	0.04621	-7.58
	Electrolyte concentration [M]	8	8.0002	0.002
	Minimum porosity of anode	0.731	0.731	0.00
	Energy Density [Wh/kg]	403.04104	494.74	22.75
	Power Density [W/kg]	200	235.59	17.80
	Discharge Time [h]	2.01521	2.1	4.21

4. Conclusion

This work presents the first comprehensive multiphysics modeling study of Ni-Fe batteries to simulate the complex interactions between various physical phenomena. A 1D isothermal multiphysics model of a Ni-Fe

battery was developed to maximize energy density and power density. Based on the experimental data of Lei et al. (2016), the developed model produced RMSE and Δmax values of 0.0417 V and 0.1225 V, to which the deviations are largely attributed to OCV deviations. The exact fit, however, is difficult to achieve due to the limited parameters available from the experimental reference. This study is limited to simple nanostructured electrodes without additives, which may further contribute to the error. The validated model was utilized to perform sensitivity analysis on design parameters with respect to energy density. Significant parameters determined include thickness, porosity, and particle size of both electrodes and electrolyte concentration. Through the COBYLA algorithm, the maximum energy density and power density were calculated by optimizing sensitive design parameters. Improvements in the 1-step case were attributed to the reduced thickness and active material loading of the anode, while reduced thickness, porosity, and active particle size of the cathode were ascribed to the 2-step case. The generated model can be extended to 2D or 3D models to capture various battery phenomena. It is also recommended to consider different battery design parameters and perform sensitivity analysis in a wider range of discharge rates.

Acknowledgments

The work is supported by the Advanced Batteries Center Program funded by the Department of Science and Technology - Niche Centers in the Regions (DOST-NICER) as part of the REBCell Project.

References

Bernard P., 2009, Secondary batteries–nickel systems. Nickel–cadmium: sealed. In: Garche J., Dyer C.K. (Eds), Encyclopedia of Electrochemical Power Source, Academic Press / Elsevier, Amsterdam, The Netherlands, DOI: 10.1016/B978-044452745-5.00154-4, 459–481.

Castro M.T., Del Rosario J.A.D., Ocon J.D., 2022, Energy Density Optimization in a Primary Alkaline Battery using Multiphysics Modeling. Chemical Engineering Transactions, 94, 301-306.

De Vidts P., White R.E., 1995, Mathematical modeling of a nickel-cadmium cell: Proton diffusion in the nickel electrode. Journal of The Electrochemical Society, 142(5), 1509–1519.

He Z., Xiong F., Tan S., Yao X., Zhang C., An Q., 2021, Iron Metal Anode for Aqueous Rechargeable Batteries. Mater. Today Adv., 11, 100156.

Jiang K., Liu X., Lou G., Wen Z., Liu L., 2020, Parameter sensitivity analysis and cathode structure optimization of a non-aqueous Li–O_2 battery model. Journal of Power Sources, 451, 227821.

Lee J., Choi K.W., Yao N.P., Christianson C.C., 1986, Three-dimensional thermal modeling of electric vehicle batteries. Journal of The Electrochemical Society, 133(7), 1286–1291.

Lei D., Lee D.-C., Magasinski A., Zhao E., Steingart D., Yushin G., 2016, Performance enhancement and side reactions in rechargeable nickel–iron batteries with nanostructured electrodes. ACS Applied Materials & Interfaces, 8(3), 2088–2096.

Linden D., Beard K.W., Reddy, T.B., 2019, Linden's handbook of batteries, 5th Ed, McGraw Hill Professional: New York, United States.

Periasamy P., Babu B.R., Iyer S.V., 1996, Cyclic voltammetry studies of porous iron electrodes in alkaline solutions used for alkaline batteries. Journal of Power Sources, 58(1), 35–40.

Rai A.K., Anh L.T., Gim J., Mathew V., Kang J., Paul B.J., Song J., Kim J., 2013, Simple synthesis and particle size effects of TiO_2 nanoparticle anodes for rechargeable lithium-ion batteries. Electrochimica Acta, 90, 112–118.

Raventos A.M., Kluivers G., Haverkort, J.W., De Jong W., Mulder F.M., Kortlever R., 2021, Modeling the Performance of an Integrated Battery and Electrolyzer System. Ind. Eng. Chem. Res., 60(30), 10988–10996.

Shukla A.K., Ravikumar M.K., Balasubramanian T.S., 1994, Nickel/iron batteries. Journal of Power Sources, 51(1-2), 29–36.

Tang H., Sun Z., Chang K., Hou Y., Li B., Hou Y., Chang Z., 2019, Uniform Carbon Coating Drastically Enhances the Electrochemical Performance of a Fe_3O_4 Electrode for Alkaline Nickel–Iron Rechargeable Batteries. Int. J. Hydrogen Energy, 44, 24895–24904.

Tsehaye M.T., Teklay Gebreslassie G., Heon Choi N., Milian D., Martin V., Fischer P., Tübke J., El Kissi N., Donten M.L., Alloin F., Iojoiu C., 2021, Pristine and modified porous membranes for zinc slurry–air flow battery. Molecules, 26(13), 4062.

Wang H., Liang Y., Gong M., Li Y., Chang W., Mefford T., Zhou J., Wang J., Regier T., Wei F., Dai H., 2012, An Ultrafast Nickel-Iron Battery from Strongly Coupled Inorganic Nanoparticle/Nanocarbon Hybrid Materials. Nat. Commun., 3, 917–918.